

Terahertz quantum-well photodetectors: Design, performance, and improvements

S. Zhang, T. M. Wang, M. R. Hao, Y. Yang, Y. H. Zhang et al.

Citation: *J. Appl. Phys.* **114**, 194507 (2013); doi: 10.1063/1.4826625

View online: <http://dx.doi.org/10.1063/1.4826625>

View Table of Contents: <http://jap.aip.org/resource/1/JAPIAU/v114/i19>

Published by the [AIP Publishing LLC](#).

Additional information on *J. Appl. Phys.*

Journal Homepage: <http://jap.aip.org/>

Journal Information: http://jap.aip.org/about/about_the_journal

Top downloads: http://jap.aip.org/features/most_downloaded

Information for Authors: <http://jap.aip.org/authors>



Re-register for Table of Content Alerts

Create a profile.



Sign up today!



Terahertz quantum-well photodetectors: Design, performance, and improvements

S. Zhang,^{a)} T. M. Wang, M. R. Hao, Y. Yang, Y. H. Zhang, W. Z. Shen, and H. C. Liu
*Department of Physics and Astronomy, Key Laboratory of Artificial Structures and Quantum Control
 (Ministry of Education), Shanghai Jiao Tong University, Shanghai 200240, China*

(Received 8 August 2013; accepted 7 October 2013; published online 21 November 2013)

Theoretical studies and numerical simulations on design, performance, and improvements of terahertz quantum-well photodetector (THz QWP) are presented. In the first part of this paper, we discuss the device band structure resulting from a self-consistent solution and simulation results. First, the temperature dependence of device characteristics is analyzed. Next, we deduce the condition of optimal doping concentration for maximizing dark current limited detectivity D_{det}^* when QWP is lightly doped. Accordingly, unlike in previously published reports, doping concentration is not fixed and is selected by the above condition. In the second part of this paper, we propose two schemes for improving operation temperature. The first is to incorporate an optical antenna which focuses incident THz wave. Numerical results show that the QWP with peak frequency higher than 5.5 THz is expected to achieve background-noise-limited performance at 77 K or above when employing a 10^6 times enhancement antenna. The second scheme is to use a laser as the signal source to achieve photon-noise-limited performance (PLIP) at high temperatures. Simulations show that when operating below critical temperature QWPs in the range of 1 ~ 7 THz can reach PLIP under practical illumination intensities. © 2013 AIP Publishing LLC. [<http://dx.doi.org/10.1063/1.4826625>]

I. INTRODUCTION

Presently, considerable interest has been paid to terahertz quantum-well photodetector (THz QWP) which is a good candidate for compact terahertz systems. Compared with other types of THz detectors, THz QWP has some unique advantages originating from characteristics of inter-subband transition and unipolar transport properties. The parameters of QWPs can be designed according to a specifically required response frequency. The fast intrinsic response speed enables high-frequency applications.¹ THz QWPs, as a natural extension of the traditional quantum-well infrared (IR) photodetector into longer wavelength region, have basically the same physical mechanism of detection and design rules. However, unlike IR QWP technology, THz QWP is far from mature and the performance needs substantial improvements. First, additional physical effects, which in the IR region can be neglected, must be included. The low value of transition energy (small response frequency) of THz QWP necessitates the inclusion of many-particle effects, which adds extra computations and uncertainties. Recently, Guo *et al.* reported a self-consistent solution using plane wave expansion by which they calculated band structure and designed parameters of device including many-particle effects.^{2,3} Second, the low barrier height results in a low background-noise-limited performance (BLIP) temperature, which seriously limits THz QWP's application scope. Moreover, our experimental results on THz QWPs with increased doping densities have showed non-trivial trends and attempts on reaching

lower THz region (<3 THz) have thus-far failed. Clearly more detailed simulations, which are the focus of this paper, and experimental work, which are on-going, are called for.

The paper is organized as follows. In Sec. II, the theoretical framework of self-consistent solution for band structure is presented. Furthermore, the temperature dependence of device characteristics is discussed. Then, a scheme using an optical antenna to increase BLIP temperature is proposed. Next, a photon-noise-limited performance (PLIP) application which utilizes a high power signal source to raise THz QWP's working temperature is described. Afterwards, we deduce the optimum doping concentration for maximizing detectivity when QWP is lightly doped. In Sec. III, we investigate numerically the various issues mentioned in Sec. II. First, on the basis of simulation given by Guo *et al.*,⁴ where doping concentration is fixed, we present an improvement which sets doping concentration as the one which maximizes detectivity D_{det}^* . Furthermore, numerical results on performance characteristics (such as BLIP temperature and PLIP regime) are given and discussed in details.

II. THEORY AND MODEL

A. Self-consistent solution of band structure

The generally accepted design rule for QWP is to ensure the first excited subband in alignment with the top of the barrier. For designing IR QWPs, the requirement is easily met since many-particle interactions are small compared with the intersubband energy and negligible for the determination of

^{a)}Electronic mail: phybuff@sjtu.edu.cn.

the first excited state. In contrast, the quantum well of THz QWP is very shallow, therefore above effects play a key role in band structures and the response peak frequency. Within the effective mass approximation, the Schrödinger equation in the quantum well growth direction z is

$$\left\{ -\frac{\hbar^2}{2} \frac{\partial}{\partial z} \left[\frac{1}{m^*(z)} \frac{\partial}{\partial z} \right] + V_{QW}(z) + V_H(z) + V_{xc}(z) \right\} \varphi_{l,kz}(z) = \varepsilon_{l,kz} \varphi_{l,kz}(z). \quad (1)$$

Here, m^* is the electron effective mass, \hbar is the reduced Planck constant, V_{QW} is the stepwise potential energy representing the conduction band offset profile, V_H is the Hartree potential energy obtained from Poisson's equation, V_{xc} is the exchange-correlation potential energy which is given by the local density approximation based on the density functional theory,^{5,6} $\varphi_{l,kz}$ is z -direction envelope function, and $\varepsilon_{l,kz}$ is eigen-energy, where l is miniband index and k_z is z -direction wavevector. Schrödinger equation and Poisson equation, along with exchange-correlation expression form a closed set which should be solved self-consistently. The self-consistency is realized by an iterative procedure until convergence is achieved.⁷ In this paper, we numerically solve above equations using a plane-wave expansion method.² In Sec. III, we use the following criteria to check the convergence: $|(E_{F(i)} - E_{F(i-1)})/E_{F(i)}| \leq 0.0001$, with $E_{F(i)}$ being the Fermi energy at the i th iterative step.²

The calculation method of Fermi energy E_F is shown below. In the band structure of QWP, each eigen-energy $\varepsilon_{l,kz}$ corresponds to a subband or an in-plane parabolic band, i.e., the total energy of electron is $E = E_{kz} + \hbar^2 k_{\parallel}^2/2m$, here k_{\parallel} is the in-plane wavevector in the x - y plane. The number of electrons on a given subband is $N_{l,kz}(E_F)$

$$N_{l,kz}(E_F) = \frac{m_{average}}{\pi \hbar^2} k_B T \ln \left[1 + \exp \left(\frac{E_F - \varepsilon_{l,kz}}{k_B T} \right) \right], \quad (2)$$

where the average electron effective mass $m_{average}$ is defined as $m_{average} = m^*_w \int_{well} |\varphi_i(z)|^2 dz + m^*_b \int_{barrier} |\varphi_i(z)|^2 dz$, m^*_w (m^*_b) is effective mass in the well (barrier), k_B is the Boltzmann constant. Hence, the summation over all subbands equals the product of 2-dimensional (2D) doping density N_{2Ddope} and period number N_{QW} (the right-hand side of below equation)

$$\sum_{l,kz} N_{l,kz}(E_F) = N_{3Ddope} L_{dope} N_{QW}. \quad (3)$$

Here, N_{3Ddope} is three-dimensional (3D) doping (usually with silicon for GaAs/AlGaAs materials system) concentration in a center region of QW, L_{dope} is doping region width, $N_{2Ddope} = N_{3Ddope} L_{dope}$. Through calculation, we find that the electron density in the lowest subband is orders of magnitude higher than that on all of the other subbands. As an approximation in our calculation, the left-hand side of Eq. (3) is replaced by a summation of 3D free electrons above the barrier and electrons of the lowest subband, i.e.,

$$N_{3D} L_{period} N_{QW} + \sum_{l=1}^1 \sum_{kz} N_{l,kz}(E_F) = N_{3Ddope} L_{dope} N_{QW}, \quad (4)$$

where quantum well period L_{period} is the sum of well width L_w and barrier thickness L_b , 3D above-barrier free electron density N_{3D} can be approximated by

$$N_{3D} = 2 \left(\frac{m^*_b k_B T}{2\pi \hbar^2} \right)^{3/2} \exp \left(-\frac{V_b - E_F}{k_B T} \right). \quad (5)$$

Here, V_b is the barrier height. Therefore, E_F is obtained by solving Eq. (4).

Of particular importance is the temperature dependence of various parameters of QWP. From Eq. (2), it is evident that temperature T directly determines subband electron number $N_{l,kz}(E_F)$ and affects electron density along z -direction $\rho_e(z)$ through Eq. (6)

$$\rho_e(z) = |e| \sum_{l,kz} N_{l,kz} |\varphi_{l,kz}(z)|^2. \quad (6)$$

Furthermore, Hartree and exchange-correlation potentials depend on electron density $\rho_e(z)$. Thus eigen-energies change with temperature T , leading to a situation that the QWP parameters (L_w , x , N_{3Ddope}) designed for one operating temperature do not best fit for another operating temperature. Therefore, it is better to design THz QWP parameters according to each specific operating temperature. However, in the situation, where it is not practical to determine the accurate operating temperature in advance, we approximately take the calculated parameters for a fixed temperature.

B. Different operation regimes

For a typical photodetector, the total current I_{total} originates from dark current carriers, background radiation generated carriers, and signal radiation generated carriers. Accordingly, I_{total} can be expressed as a summation of the above three contributions

$$I_{total} = I_{dark} + RP_B + RP_S. \quad (7)$$

Here, R is detector responsivity, P_B is background radiation power, P_S is signal radiation power. According to the relative magnitudes among RP_S , RP_B , and I_{dark} , the operating status of QWP can be categorized into three performance regimes:¹ PLIP in which RP_S dominates, BLIP in which RP_B dominates, and dark-current-limited performance in which I_{dark} dominates. In order to achieve maximal sensitivity, it is always desirable to operate a QWP under BLIP or PLIP conditions. In standard theory of QWP, the dark current mainly comes from thermal excitation when electric field is small and quantum barrier is thick (so we can neglect the contribution from scattering assisted tunneling and inter-well tunneling).

$$J_{dark} = e N_{3D} \nu_{drift}(F), \quad (8)$$

where $\nu_{drift}(F)$ is the drift velocity as a function of electric field F , and N_{3D} is given by Eq. (5). Photocurrent density generated by a monochromatic light (e.g., a laser) is given by

$$J_{photon}(\nu) = e\phi(\nu)\eta(\nu)g, \quad (9)$$

where ν is frequency, $\Phi(\nu)$ is photon number flux, $\eta(\nu)$ is absorption efficiency, and photoconductive gain $g \approx \tau_c \nu_{drift}(F)/N_{QW}L_{period}$, where τ_c is the excited carrier capture time. If the incident radiation is broadband, such as from blackbody radiation, we should use the integrated background photon number flux $\Phi_{B,ph}$.¹

$$J_{photon_broadband} = e\phi_{B,ph}\eta^{(1)}N_{QW}g, \quad (10)$$

where $\eta^{(1)}$ is peak absorption efficiency of single well and double pass, $\eta^{(1)} \propto N_{2Ddope}/\Delta E$ (ΔE is full width at half maximum (FWHM) of absorption spectrum, where horizontal axis is energy, i.e., $\Delta E = 2 \times (h\nu_p - h\nu_c)$, here, ν_p is peak response frequency, ν_c is cutoff frequency).¹ According to some reported THz QWPs of V266, V267, and M570,^{3,8} we find the simple empirical relation among $\eta^{(1)}$ and N_{2Ddope} and $h\nu_p$: $\eta^{(1)} = C \times N_{2Ddope}/\Delta E$, where $C = 4.05 \times 10^{-13}$, $\Delta E = 0.25 \times h\nu_p$ (the units of N_{2Ddope} and ΔE are cm^{-2} and meV, respectively). In addition, we give calculated absorption coefficient to verify above empirically fitted model. Absorption efficiency η is given by¹

$$\eta = \frac{e^2 h}{4\epsilon_0 n_r m_w^* c} \frac{\sin^2 \theta}{\cos \theta} N_{2Ddope} f \frac{1}{\pi} \frac{\Gamma}{(h\nu - E_{21})^2 + \Gamma^2}, \quad (11)$$

where ϵ_0 is vacuum permittivity, the refractive index is 3.3, the angle between THz ray's propagating direction and QW's growth axis θ is 45° , the Lorentzian linewidth constant $\Gamma = \Delta E/2$, the oscillator strength $f = \frac{4\pi m_w^* v}{h} |\langle \varphi_2 | z | \varphi_1 \rangle|^2$, and φ_2 and φ_1 are the first excited and the ground state z-direction wavefunctions, respectively. Through comparing two formulas of η , the constant C is given by $C = \frac{e^2 h}{4\epsilon_0 n_r m_w^* c} \frac{\sin^2 \theta}{\cos \theta} f \frac{2}{\pi}$. We choose QWP V267 to compute absorption coefficient. V267's parameters are as follows: $L_w = 22.1$ nm, $Al_x = 1.5\%$, and $N_{3Ddope} = 3 \times 10^{22} \text{ m}^{-3}$. Through calculating integral of the wavefunctions, we obtain that oscillator strength $f = 0.9064$ and $C = 4.0527 \times 10^{-13}$, which is very close to our empirical value (note that we have doubled it because $\eta^{(1)}$ means double pass absorption efficiency). The comparison result shows that our empirically fitted model is acceptable. Therefore, we use the model to obtain peak absorption efficiency for other QWP with different doping density and peak response frequency.

1. BLIP temperature with an antenna

In many applications of QWP, such as passive thermal imaging, signal radiation is very weak. Correspondingly, signal current is negligible compared with background current and dark current. To achieve optimal performance, the operation temperature should be lowered sufficiently to suppress dark current until the background current dominates. Then, QWP is said to be under BLIP regime if operated below

T_{blip} , and the critical temperature is determined when J_{dark} equals J_{photon} . Due to the low barrier height of THz QWP and the fact that thermally excited dark current increases exponentially when barrier height decreases, the BLIP temperature T_{blip} of THz QWP is quite low (below 30 K for 7 THz QWP),^{9,10} which seriously limits its application.

In this paper, we analyze the situation, where the dimensions of QWP are reduced in order to suppress dark current and improve BLIP temperature. However, terahertz wave's long wavelength determines the device's minimum dimension, below which the absorption will be insufficient. The common solution is using an antenna, which can couple the incident light efficiently and concentrate the far-field radiation into small localized areas.^{11,12} Therefore, when equipped with a THz antenna, QWP dimension is allowed to decrease to micrometer scale. Here, we focus on the improvement of T_{blip} with an antenna and give an ideal estimation on antenna enhancement as follows. The inset of Figure 4 shows a schematic of the optical-antenna-coupled THz QWP. We suppose the antenna dimension to be $100 \times 100 \mu\text{m}$ and the QWP dimension to be $1 \times 1 \mu\text{m}$. Assuming that antenna can ideally capture and focus $100 \times 100 \mu\text{m}$ size incident THz ray into $1 \times 1 \mu\text{m}$ size QWP, the photon number flux Φ increases 10^4 times with the antenna. In an extreme case, we may shrink the QWP size to $0.1 \times 0.1 \mu\text{m}$ (the length of n-type GaAs surface depletion) with an enhancement factor as large as 10^6 . In the following analyses, we denote the antenna enhancement factor as $K_{antenna}$. From Eqs. (8) to (10), we deduce the following equations:

$$\eta^{(1)} \tau_c \phi_{B,ph} = 2 \left(\frac{m_b k_B T}{2\pi \hbar^2} \right)^{3/2} L_{period} \exp\left(-\frac{V_b - E_F}{k_B T}\right), \quad (12)$$

$$\eta^{(1)} \tau_c \phi_{B,ph} K_{antenna} = 2 \left(\frac{m_b k_B T}{2\pi \hbar^2} \right)^{3/2} L_{period} \times \exp\left(-\frac{V_b - E_F}{k_B T}\right). \quad (13)$$

Solving Eqs. (12) and (13) for temperature gives T_{blip} without and with antenna, respectively.

2. Required power for PLIP regime

Certain applications (e.g., gas sensing and heterodyne detection) require the combined use of a QWP, and a laser (such as a quantum cascade laser—QCL) which acts as either the source or local oscillator. These applications are rapidly emerging since THz QCLs can provide high power up to hundreds of milliwatts. Using a high-power THz QCL as the signal radiation source, signal current can be larger than dark current and background photocurrent at operating temperatures higher than T_{blip} . We define the regime where signal current dominates as PLIP. Figure 5(a) shows combined use of a QCL and a THz QWP. The required threshold power and flux when signal photocurrent equals the dark current are called $power_{plip}$ and $flux_{plip}$, respectively, which can be obtained by solving Eqs. (8) and (9).

$$flux_{plip} = \frac{N_{3D}L_{period}}{\tau_c\eta^{(1)}}, \quad (14a)$$

$$power_{plip} = h\nu_p \frac{N_{3D}L_{period}}{\tau_c\eta^{(1)}}. \quad (14b)$$

C. Optimum doping concentration for maximizing dark-current limited detectivity

The general expression of dark-current limited detectivity D_{det}^* is

$$D_{det}^* = \frac{\lambda}{2hc} \frac{\eta}{\sqrt{N_{QW}}} \sqrt{\frac{\tau_c}{N_{3D}L_p}}. \quad (15)$$

The widely used optimum condition of doping concentration (or Fermi energy) for maximizing dark-current limited detectivity D_{det}^* is $E_F = 2k_B T$.¹ The condition is deduced within the assumption that the quantum well layers of QWP are heavily doped n-type GaAs, and the formula for subband electron density Eq. (2) is simplified as $n_{2D} = E_F \times m/(\pi\hbar^2)$. However, for the lightly doped THz QWP, the above approximation is not applicable anymore. We therefore need to look at the following: $D_{det}^* \propto \eta \sqrt{\frac{1}{N_{3D}}} \propto n_{2D} e^{-\frac{E_F}{2k_B T}}$

$\propto \ln(e^{\frac{E_F}{k_B T}} + 1) e^{-\frac{E_F}{2k_B T}}$, where the zero point of potential energy is set at ground subband. The optimum doping concentration (or Fermi energy) is deduced by $\frac{d}{d(\frac{E_F}{k_B T})} [\ln(e^{\frac{E_F}{k_B T}} + 1) e^{-\frac{E_F}{2k_B T}}] = 0$.

Above condition gives $E_F/(k_B T) = \ln(-2/lambertw(0, -2 \times 10^{-2}) - 1) \approx 1.3665$, where *lambertw* denotes Lambert *W* function, (also called the omega function) which is the inverse function of $f(W) = We^W$. So the following condition guarantees the maximum D_{det}^* where T is the desired operation temperature.

$$E_F = 1.3665 \times k_B T. \quad (16a)$$

In most case, operation temperature roughly equals BLIP temperature T_{blip} , so

$$E_F \approx 1.3665 \times k_B T_{blip}. \quad (16b)$$

Putting Eq. (16) into Eq. (4), we obtain the optimum doping concentration for a given operating temperature T or T_{blip} .

$$N_{2Ddope_best} = \frac{m_w^*}{\pi\hbar^2} k_B T \ln(e^{1.3665} + 1) = 1.59 \frac{m_w^*}{\pi\hbar^2} k_B T, \quad (17)$$

where we have neglect the first excited subband electrons and 3D-electrons terms in Eq. (4) (which is a commonly used approximation¹).

III. CALCULATION AND DISCUSSION

A. Self-consistent solution of band structure

The band structure of an n-type GaAs-AlGaAs QWP is determined by the following physical quantities: quantum well width L_w , barrier aluminum fraction x , and quantum well doping concentration N_{3Ddope} (when doping width is fixed). First, we present calculation examples to show the significance of many-body effects (by including Hartree potential energy V_H , exchange-correlation potential energy V_{xc} , and depolarization energy $E_{depolar}$ ² step by step). We choose two QWPs from Fig. 3's results to calculate their band structures without and with considering many-body effects. In Table I, the two QWPs' results show that many-body effects decrease ground state energy E_1 by 4~5 meV and increase response peak frequency ν_p by 0.8~1 THz, which indicates that many-body effects indeed play an important role in the design of terahertz QWPs.

Guo *et al.* calculated response peak frequencies in QWP parameter space of $x = 0.5\% \sim 4.0\%$ and $L_w = 10 \sim 30$ nm without and with considering the many-particle interactions.⁴ The silicon doping concentration in quantum well N_{3Ddope} was fixed to $4 \times 10^{16} \text{ cm}^{-3}$. Similarly, we first calculate QWP parameters with fixed doping concentration. Figure 1 illustrates the calculated well width and aluminum fraction for corresponding response peak frequencies at 8 K and 77 K. In our simulation, the parameters are as follows: aluminum fraction $x = 0.1\% \sim 8\%$, $L_w = 10 \sim 25$ nm, $N_{3Ddope} = 4 \times 10^{16} \text{ cm}^{-3}$, doping width L_{dope} is 10 nm in the central region of the quantum well, the number of QW periods N_{QW} is 30, the barrier height $V_b = x \times 0.87 \text{ eV}$ and the barrier thickness L_b is sufficiently thick so that the inter-well tunneling can be neglected (here, we set it as $L_b = 4.5 \times L_w$). 150 plane waves are used to expand the envelope wave functions.² As shown, the two curves overlap at high frequency region ($\nu > 3$ THz), and we can therefore neglect the temperature effects. In contrast, for the lower frequency range, the obvious differences between

TABLE I. Comparison of eigen-energies and response peak frequencies with and without including many-body effects. The two QWPs are chosen from Fig. 3's results. The temperature is 10 K.

QWP sample	L_w (nm)	Al _x (%)	N_{3Ddope} (m^{-3})	Without considering many-body effects			Considering V_H and V_{xc}			
				E_1 (meV) ^a	E_2 (meV) ^b	ν_p (THz) ^c	E_1 (meV) ^a	E_2 (meV) ^b	ν_p (THz) ^c	
									Not considering $E_{depolar}$	Considering $E_{depolar}$
1	12.9	3.4	5.74×10^{22}	10.87	29.98	4.62	5.36	28.05	5.48	5.67
2	16.7	1.9	3.36×10^{22}	6.33	16.85	2.54	2.02	15.43	3.24	3.38

^a E_1 is ground state energy.

^b E_2 is first excited state energy.

^c ν_p is response peak frequency.

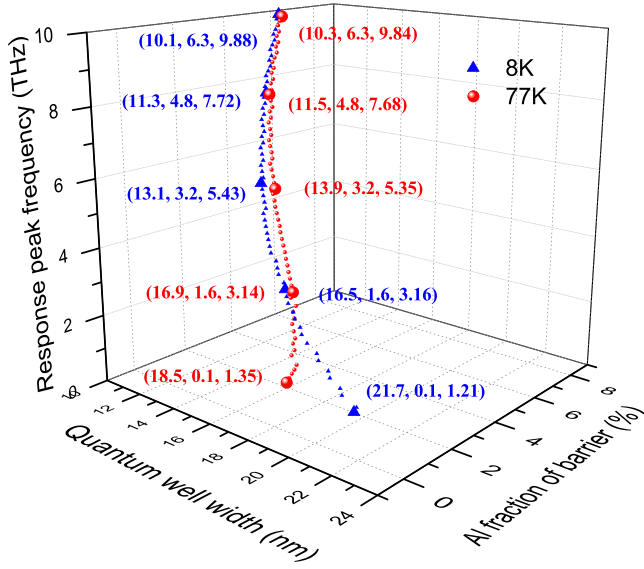


FIG. 1. Calculated quantum well width and aluminum fraction for corresponding response peak frequency at 8 K and 77 K. $N_{3Ddope} = 4 \times 10^{16} \text{ cm}^{-3}$. In the simulation, we include V_H , V_{xc} , and $E_{depolar}$.

two curves indicate that the influence of operating temperature should be taken into consideration.

Now, we calculate the band structure letting L_w , x , and N_{3Ddope} as free parameters. Figure 2 shows the calculated combinations of parameters for 4 THz QWP. In our simulation, the parameters are as follows: aluminum fraction $x = 1.7\% \sim 2.4\%$, $L_w = 14.9 \sim 15.5 \text{ nm}$, $N_{3Ddope} = 2 \sim 7 \times 10^{16} \text{ cm}^{-3}$, the temperature T is 10 K, other values are the same as in Figure 1. The energy difference between the top of barrier and the first excited subband should be less than 2.0 meV,⁴ so that excited electrons in the first subband can escape efficiently. In our simulation, the calculated parameters in Figure 2 correspond to an energy difference about 1 meV, which satisfies the design rule well.

When doping concentration N_{3Ddope} increases, on the one hand, absorption efficiency and signal current will be enhanced. On the other hand, many-particle effects become stronger and eigenenergies falls more deeply.² To satisfy design rule, aluminum fraction has to be decreased (as the curve shown in Fig. 2(a)) resulting in an exponential increase of dark current. So there is a trade-off in the selection of doping concentration: weighing the benefits of improving photocurrent against the unwanted enhancement of dark current. Since each dot from Fig. 2(a) curve represents a set of three parameters (L_w , x , N_{3Ddope}) which ensure the first excited subband in resonance with the top of the barrier, we can choose one dot (3 parameters) which optimizes a specific figure-of-merit. The figure-of-merit should contain information characterizing absorption efficiency and dark current simultaneously in order to solve the dilemma stated above. Here, we select QWP parameters which maximize D_{det}^* (i.e., doping concentration equals N_{3Ddope_best} in Eq. (17)). From Eq. (17), first we need to obtain the BLIP temperature T_{blip} . As a rough estimation, T_{blip} linearly depends on response frequency,¹³ i.e., $T_{blip} = c \times \nu$, where ν is response frequency and c is a constant. The upper curve and lower curve in Figure 1 of Ref. 13

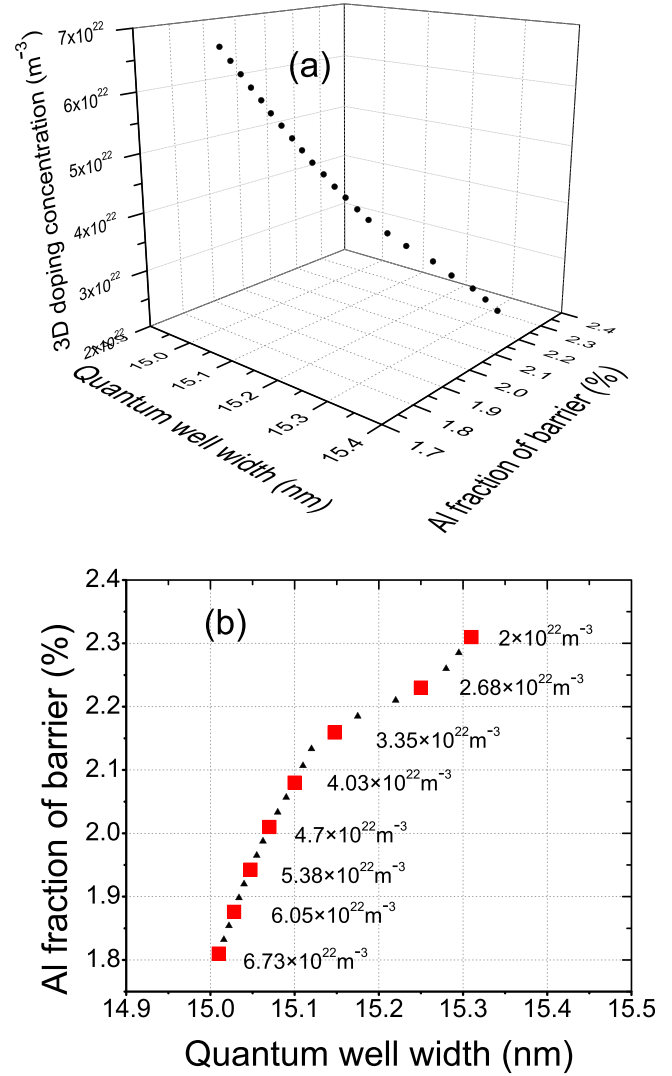


FIG. 2. Calculated quantum well width, aluminum fraction, and doping concentration for 4 THz QWP. (a) Three-dimension plot. (b) Two-dimension plot. The value nearby the red dot represents the corresponding doping concentration (the red dots are randomly chosen from the black dots, i.e., they are all simulated results). The temperature T is 10 K. In the simulation, we include V_H , V_{xc} , and $E_{depolar}$.

correspond to different ratios c with different doping concentrations. Therefore, in order to obtain the N_{3Ddope_best} , it is necessary to calculate N_{3Ddope_best} 's corresponding ratio c . The procedure is presented briefly: taking the 4 THz (there is a weak correlation between QWP parameters and temperature T around 4 THz from Figure 1) QWP parameters from Figure 2, through Eq. (12) we obtain a T_{blip} for every QWP (the numerical calculation of T_{blip} will be elaborated in Sec. III B). Then, through Eq. (17) we get the optimum doping concentration N_{3Ddope_best} corresponding to every QWP with parameters L_w , x , and N_{dope} . Next, we find the parameters which have the minimum difference between N_{3Ddope_best} and N_{dope} : $L_w = 15.1 \text{ nm}$, $x = 2.08\%$, $N_{dope} = 4.03 \times 10^{16} \text{ cm}^{-3}$, $T_{blip} = 10.3 \text{ K}$. Finally, we determine the ratio: $c = 10.3 / (4 \times 10^{12})$. Putting $T_{blip} = c \times \nu$ into Eq. (17), we can improve the simulation reported by Guo *et al.*⁴ with doping concentration obeying the condition $N_{dope} = \frac{1.59 m_w^*}{L_{dope} \pi \hbar^2} k_B c \nu$, which only contains variable ν .

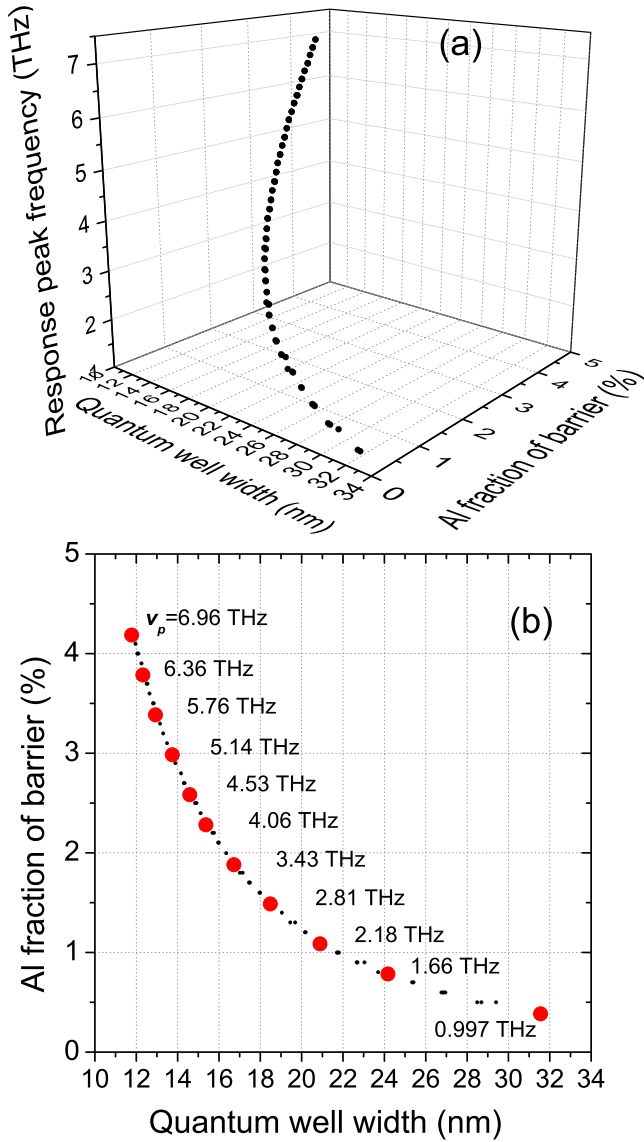


FIG. 3. Calculated quantum well width and aluminum fraction for a given response peak frequency. The doping concentration is selected by $N_{2Ddope} = 1.59 \frac{m_w^*}{\pi \hbar^2} k_B c v$, here $c = 10.3/(4 \times 10^{12})$. The parameters here guarantee maximal dark current limited detectivity D_{det}^* . (a) Three-dimension plot. (b) Two-dimension plot. The value around the red dot represents the response peak frequency (the red dots are randomly chosen from the black dots, i.e., they are all simulated results). In the simulation, we include V_H , V_{xc} , and $E_{depolar}$.

Figure 3 shows the calculated quantum well widths and aluminum fractions for different response frequencies with optimum doping concentration. In our simulation, the parameter ranges are: aluminum fraction $x = 0.1\% \sim 5.7\%$, $L_w = 10 \sim 34$ nm, response frequency is $1 \sim 7$ THz, $N_{3Ddope} = \frac{1.59}{L_{dope}} \frac{m_w^*}{\pi \hbar^2} k_B c v$, where $c = 10.3/(4 \times 10^{12})$, other values are the same as in Figure 2.

B. Different performance regimes

1. BLIP temperature with an antenna

Figure 4 illustrates the calculated BLIP temperature T_{blip} for different peak detection frequencies ν_p by solving Eqs.

(12) and (13). As shown, the simulated T_{blip} without antenna enhancement is consistent with calculated and experimental results reported before.^{13,14} Approximately, BLIP temperature depends linearly with peak frequency. Comparing the five curves shown in the figure, incorporating optical antennas indeed improve BLIP temperature. However, significant rise can only be achieved by a high order focusing antenna (a 10^6 times enhancement antenna gives a fivefold T_{blip} , a 10^4 times enhancement antenna gives a doubled T_{blip} , a 10^2 times enhancement antenna only increases T_{blip} by 5 K for a 4 THz QWP). Theoretically, it is anticipated that the QWP with peak frequency higher than 5.5 THz may operate at BLIP performance at 77 K or above when employing a 10^6 times enhancement antenna. It is important to note that BLIP temperature does not continue to increase when the focusing capacity of antenna becomes higher and higher. Since when operating temperature rises, 3D above-barrier free electrons count for a growing part of the whole doping electrons. So we need to make sure the proportion of 3D electrons less than a certain percentage (here, we set it as 10%) to guarantee, there are still enough bound state electrons which are used for generating photocurrent. Then, we get each QWP's corresponding critical operating temperature, which is 16 K for 1 THz QWP, 62.5 K for 4 THz QWP, and 107 K for 7 THz QWP. As Fig. 4 shows, when antenna enhancement factor is 10^6 , T_{blip} is below critical operating temperature for each QWP, so all of the results of BLIP temperatures in Fig. 4 make sense.

In the calculation, typical values are used with 90° field-of-view and 300 K background temperature. Barrier effective mass m_b , QW period thick L_{period} , doping concentration N_{3Ddope} , and response peak frequency ν_p are taken from Figure 3. Fermi energy E_F follows the rule: $E_F = 1.3665 \times k_B T$ (it is also verified by calculation results of Fermi energy). In addition, we assume peak absorption efficiency (single well

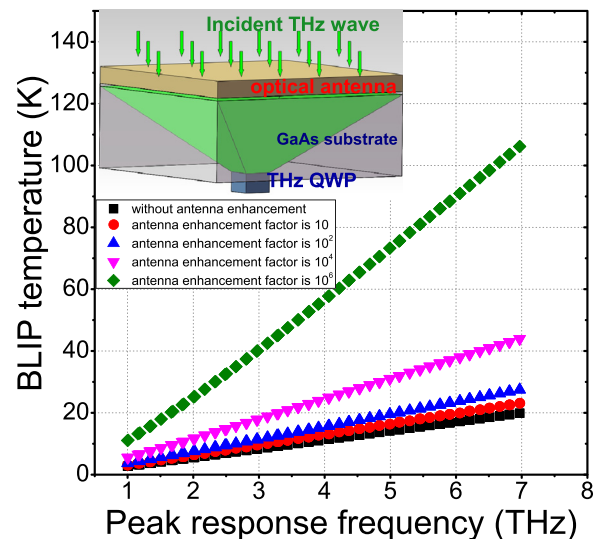


FIG. 4. Calculated BLIP temperatures for different peak response frequencies with or without optical antenna. Background temperature is 300 K, FOV is 90° , lifetime $\tau_c = 10$ ps. QWP parameters are taken from Figure 3, so Fermi energy follows $E_F = 1.3665 \times k_B T$. The inset depicts the schematic of an optical-antenna-coupled THz QWP.

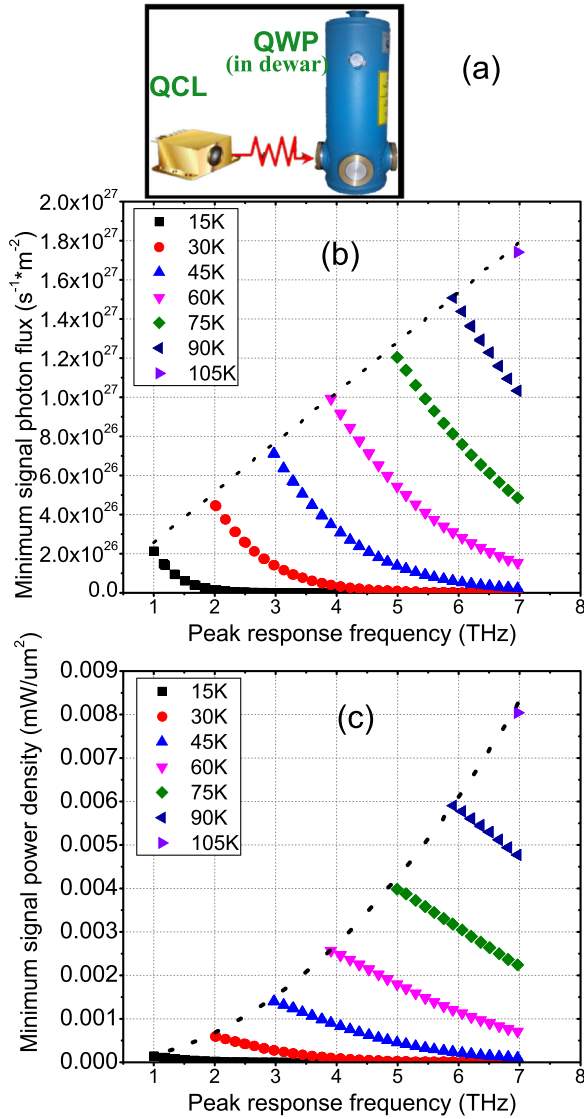


FIG. 5. (a) Illustration of combined use of a QCL and a THz QWP. (b) Minimum photon flux required for PLIP performance at different operating temperatures. (c) Minimum signal power density required for PLIP performance at different operating temperatures. The black dot curve in (b) and (c) represents the corresponding photon flux and signal power for each QWP when the QWP works at its critical operating temperature. Lifetime $\tau_c = 10$ ps. QWP parameters are taken from Figure 3, so Fermi energy follows $E_F = 1.3665 \times k_B T$.

and double pass) as $\eta^{(1)} = C \times N_{2Ddope} / (0.25 \times h\nu_p)$, where $C = 4.05 \times 10^{-13}$. Background photon number flux $\Phi_{B,ph}$ is the integral of the product of blackbody spectral lineshape and Lorentzian spectral response function with respect to frequency ν (the lower and upper limit of the integral are $\nu_p - 2 \times \Delta\nu$ and $\nu_p + 2 \times \Delta\nu$). Here, ν_p is peak response frequency, $\Delta\nu = 2 \times (\nu_p - \nu_c) = \Delta E/h$.¹ For MIR QWP, the lifetime of the excited-electron τ_c is mainly determined by optical phonon scattering rate. However, in THz region, where inter-subband transition energy E_{12} ($E_{12} = h \times \nu_p$) is smaller than LO phonon energy of GaAs (36 meV), electron-electron scattering becomes the dominant mechanism.^{15,16} From Eqs. (12) and (13), τ_c is not in the exponent. As a consequence, a small deviation of estimation of τ_c has a weak influence on the calculated result of T_{blip} . Here, the lifetime is set as $\tau_c = 10$ ps.

2. Required power for PLIP regime

Substituting the calculated data from Figure 3 into Eqs. (14a) and (14b), the relationship between minimum signal power (flux) required for PLIP performance and peak frequency ν_p is obtained. The values used in calculation are the same as Sec. III B 1: $E_F = 1.3665 \times k_B T$, $\tau_c = 10$ ps, $\eta^{(1)} = C \times N_{2Ddope} / (0.25 \times h\nu_p)$, where $C = 4.05 \times 10^{-13}$.

The minimum photon flux required for PLIP regime at different operating temperatures is plotted in Figure 5(b). The required photon flux goes up rapidly when response frequency decreases, indicating that the PLIP operating condition is more demanding at lower THz region. The results conform to our intuition that lower THz QWP has lower barrier and higher dark current, and hence needs larger photon flux. Also note that there is a black dot curve which represents the corresponding photon flux for each QWP when the QWP works at its critical operating temperature. The critical operating temperature is determined by the same way as Sec. III B 1.

Using Eq. (14a) to calculate photon flux of critical operating temperature, we obtain the black dot curve in Fig. 5(b). Figure 5(c) presents the PLIP's minimum required signal power curve which is less steep than photon flux curve due to the diminution of photon energy $h\nu$ in lower frequency region. And by similar way, we get the black dot curve, which represents the corresponding signal power for each QWP at its critical operating temperature. QWP's tolerable illumination density reported before is $0.1 \text{ mW}/\mu\text{m}^2$ on a $10 \times 10 \mu\text{m}^2$ active-area device.¹⁷ Such a high illumination density can be obtained by a high power THz QCL and a focusing optical antenna. As Fig. 5(c) shows, the required signal power is far less than $0.1 \text{ mW}/\mu\text{m}^2$ in the frequency region from 1 THz to 7 THz, indicating that the combined use of THz QWP and THz QCL for gas sensing and other applications is practical when QWP operates below critical temperature. For example, when a 4 THz QWP operates at 60 K (less than its critical temperature of 62.5 K), it needs signal power higher than $0.0025 \text{ mW}/\mu\text{m}^2$ to achieve PLIP. Note that presently THz QCLs still need cooling,¹⁸ which are compatible with the operation of THz QWPs.

IV. CONCLUSION

In conclusion, we present theoretical analyses and detailed simulations on design, performance, and improvements of THz QWPs. In the first part of this paper, discussions and calculations about device design are given. First, the temperature dependence of device characteristics is discussed. Next, we deduce the condition of optimal doping concentration for maximizing dark current limited detectivity D_{det}^* when QWP is lightly doped. Accordingly, unlike in previously published reports, doping concentration is not fixed and is selected by the above condition. Since a lower T_{blip} is the main factor limiting the application of THz QWPs, in the second part of this paper, we propose two schemes for improving operation temperature. First, a scheme that using an optical antenna to increase BLIP temperature is proposed. The calculation shows a QWP with peak frequency higher than 5.5 THz is expected to achieve

BLIP at 77 K or above when employing a 10^6 times enhancement antenna. Second, PLIP which utilizes a high-power signal to raise THz QWP's working temperature is described. The simulation results demonstrate that when operating below critical temperature QWPs in the range of $1 \sim 7$ THz can reach PLIP under practical illumination intensities.

ACKNOWLEDGMENTS

This work was supported in part by the National Major Basic Research Projects (2011CB925603), the 863 Program of China (2011AA010205), Natural Science Foundation of China (91221201, 61234005, and 11074167) and China Postdoctoral Science Foundation General Financial Grant (No. 2012M520890).

¹H. Schneider and H. C. Liu, *Quantum Well Infrared Photodetectors: Physics and Applications* (Springer, 2007).

²X. G. Guo, Z. Y. Tan, J. C. Cao, and H. C. Liu, *Appl. Phys. Lett.* **94**, 201101 (2009).

³X. G. Guo, R. Zhang, H. C. Liu, A. J. S. Thorpe, and J. C. Cao, *Appl. Phys. Lett.* **97**, 021114 (2010).

⁴X. G. Guo, J. C. Cao, R. Zhang, Z. Y. Tan, and H. C. Liu, *IEEE J. Sel. Top. Quantum Electron.* **19**, 8500508 (2013).

⁵O. Gunnarsson and B. I. Lundqvist, *Phys. Rev. B* **13**, 4274 (1976).

⁶J. Zhang and W. Pötz, *Phys. Rev. B* **42**, 11366 (1990).

⁷S. Barbieri, F. Beltram, and F. Rossi, *Phys. Rev. B* **60**, 1953 (1999).

⁸M. Graf, E. Dupont, H. Luo, S. Haffouz, Z. R. Wasilewski, A. J. S. Thorpe, D. Ban, and H. C. Liu, *Infrared Phys. Technol.* **52**, 289 (2009).

⁹H. Schneider, H. C. Liu, S. Winnerl, C. Y. Song, M. Walther, and M. Helm, *Opt. Express* **17**, 12279 (2009).

¹⁰H. Schneider, H. C. Liu, S. Winnerl, C. Y. Song, O. Drachenko, M. Walther, J. Faist, and M. Helm, *Infrared Phys. Technol.* **52**, 419 (2009).

¹¹P. Liu, W. Cai, L. Wang, X. Zhang, and J. Xu, *Appl. Phys. Lett.* **100**, 153111 (2012).

¹²A. Berrier, P. Albella, M. A. Poyli, R. Ulbricht, M. Bonn, J. Aizpurua, and J. G. Rivas, *Opt. Express* **20**, 5052 (2012).

¹³H. C. Liu, C. Y. Song, A. J. S. Thorpe, and J. C. Cao, *Appl. Phys. Lett.* **84**, 4068 (2004).

¹⁴H. Luo, H. C. Liu, C. Y. Song, and Z. R. Wasilewski, *Appl. Phys. Lett.* **86**, 231103 (2005).

¹⁵J. H. Smet, C. G. Fonstad, and Q. Hu, *J. Appl. Phys.* **79**, 9305 (1996).

¹⁶K. Kálna, M. Moško, and F. M. Peeters, *Appl. Phys. Lett.* **68**, 117 (1996).

¹⁷H. C. Liu, R. Dudek, A. Shen, E. Dupont, C. Y. Song, Z. R. Wasilewski, and M. Buchanan, *Appl. Phys. Lett.* **79**, 4237 (2001).

¹⁸S. Fatholouloumi, E. Dupont, C. W. I. Chan, Z. R. Wasilewski, S. R. Laframboise, D. Ban, A. Mátyás, C. Jiruschek, Q. Hu, and H. C. Liu, *Opt. Express* **20**, 3866 (2012).